Synthesis and characterization of a new magnetic adsorbent for removal of 4-nitrophenol: application of response surface methodology

Reza Gholamnia, Mehrnoosh Abtahi, Reza Saeedi and Shokooh Sadat Khaloo

ABSTRACT

Magnetic modified graphene oxide was synthesized as a new modified magnetic nano-composite (MMNC) by a simple sonochemical–hydrothermal method. The sonochemical reaction was employed to exfoliate, functionalize and decorate neomycin on graphene oxide sheets. Nickel ferromagnetic particles were synthesized by hydrothermal co-precipitation method and decorated on neomycin-modified graphene oxide. The morphology and chemical structure of MMNC were characterized by scanning electron microscopy, energy dispersive spectroscopy and X-ray diffraction spectroscopy. The adsorption capability of MMNC for removal of phenolic compounds was assessed through adsorption of 4-nitrophenol (4-NP) from aqueous solution. The three-factor Box–Behnken design coupled with response surface method was applied to evaluate and optimize the important variables which affect the adsorption process. A significant quadratic model (p-value <0.05, $R^2_{(adj)} = 0.9593$) was derived using analysis of variance. The maximum adsorption capacity of 125.4 mg 4-NP/g MMNC at pH 6 was obtained, which was comparable in some cases and higher than most adsorbents reported in the literature. The presence of neomycin on graphene oxide sheets improved the maximum adsorption capacity of the nano-sorbent up to 28% (from 98.7 to 125.4 mg 4-NP/g adsorbent). The adsorption isotherms fitted well with the Langmuir model (Langmuir constant $b = 0.064$ l/mg, $R^2 = 0.9989$) and the kinetic study showed that the nitrophenol uptake process followed the pseudo-second-order rate expression ($R^2 \geq 0.9960$, pseudo-second-order constant $K_2 \geq 1.7 \times 10^{-3}$).

Key words | 4-nitrophenol, graphene oxide, magnetic, removal, response surface method

Reza Gholamnia
Mehrnoosh Abtahi
Reza Saeedi
Shokooh Sadat Khaloo (corresponding author)
Workplace Health Promotion Research Center,
Shahid Beheshti University of Medical Sciences,
Tehran,
Iran
E-mail: *sh_khaloo@sbmu.ac.ir*

Reza Gholamnia
Reza Saeedi
Shokooh Sadat Khaloo
Department of Health, Safety, and Environment,
School of Public Health and Safety,
Shahid Beheshti University of Medical Sciences,
Tehran,
Iran

Mehrnoosh Abtahi
Department of Environmental Health Engineering,
School of Public Health and Safety,
Shahid Beheshti University of Medical Sciences,
Tehran,
Iran

INTRODUCTION

Nitrophenol is one of the phenolic derivatives that extensively is used in the organic synthesis and production of pharmaceuticals, polymers, fungicides, pesticides and dyes and also to darken leather. Phenol and phenolic compounds are known for their hazardous effects on the environment and humans (Khaloo *et al.* 2015). The US Environmental Protection Agency (US EPA) has listed nitrophenol (NP) compounds as the most toxic pollutants due to their excellent solubility in water and high toxicity (US EPA 2017). Most phenolic compounds such as chlorophenols, aminophenols, chlorocatechols, NPs, methylphenols and other phenolic compounds have all been characterized as exerting toxic influence on humans. These compounds can easily penetrate the skin through absorption and can readily be absorbed from the gastrointestinal tract of humans. Once in the system, they undergo metabolism and transform to various reactive intermediate forms, particularly quinone moieties, which can easily form covalent bonds with proteins, resulting in their ability to exert toxic effects on humans (William *et al.* 2017). Due to the wide application of NP compounds and hence their widespread production, disposal of these materials in aquatic systems causes severe environmental problems.

Various technologies have been used for the removal of organic or inorganic pollutant from wastewater and groundwater including electrochemical removal (Pedersen *et al.*

doi: 10.2166/wst.2019.390

2018), advanced oxidation process (Sivagami *et al.* 2018), coagulation (Abtahi *et al.* 2017; Gholami *et al.* 2017), ion exchange (López-Ortiz *et al.* 2018), precipitation (Silva *et al.* 2017), photocatalysis (Sharma *et al.* 2019) and adsorption (Yang *et al.* 2018). Among them, the adsorption technique has attracted huge attention in water treatment due to high removal efficiency without yielding harmful by-product (Naddafi *et al.* 2016; Nasseri *et al.* 2018). In the last decade, some novel adsorbents have been introduced for the adsorptive removal of organic and inorganic pollutants from aqueous environment, such as metal organic frameworks (Saedi & Roushani 2018), biomass (Altowayti *et al.* 2019), carbon-based nanomaterials (Khaloo *et al.* 2016) and alumina (Pham *et al.* 2018; Chu *et al.* 2019; Pham *et al.* 2019). Recently magnetic nano-adsorbent has gained increasing research in adsorptive water treatment techniques since the separation process could be done by applying an external magnet without filtration or centrifugation. Rapid mass transfer can be obtained due to the nano-sized structure of adsorbent having a large surface area for adsorption of analytes and, hence, facilitating the rapid adsorption equilibrium (Khaloo & Fattahi 2014).

Graphene, a two-dimensional carbon nanostructure, has attracted numerous investigations due to its unique chemical, physical and mechanical properties and a wide range of graphene-based nanomaterials have been studied and applied in various fields (Kaur *et al.* 2018). The combination of graphene and magnetic nano-particles offers magnetic graphene nano-composites as new material and provides new ways to develop novel catalysts, electrode materials and adsorbents (Hu *et al.* 2017; Liu *et al.* 2017; Rashidi Nodeh *et al.* 2017; Yang *et al.* 2017).

Recently, considerable attention has been directed towards the metal ferrite spinel compounds of the type MFe_2O_4 (M = Mn, Ni, Co, Cu, Zn). Ferrite spinel compounds are well-known magnetic materials with high magnetic permeability, large expansion coefficient, low magnetic transition temperature, high adsorption capacities, and low magnetic losses and with a wide potential application in water and wastewater treatment (Kefeni *et al.* 2017). With a combination of graphene oxide nanosheets and ferrite spinel compounds, new composites of nanomaterials have been launched which have the benefits of these two groups together. Therefore in recent years, graphene-based magnetic compounds have been shown to have a wide application in remediation of the environment (Li *et al.* 2018; Sherlala *et al.* 2018).

Different methods could be used to study the effect of various chemico-physical parameters on the efficiency of a process in chemistry. Central composite design (CCD) coupled with response surface method (RSM) is one of the useful methods for optimizing the important variables affecting a process. RSM has been applied to many purification processes such as coagulation process (Adesina *et al.* 2019), electrochemical process (Sharma & Simsek 2020), adsorptive removal (Gadekar & Ahammed 2019) and photo-Fenton oxidation (Abd Manan *et al.* 2019). CCD is a very efficient technique, providing much information on experiment variable effects and overall experimental error in a minimum number of required runs, while RSM is a collection of statistical and mathematical techniques based on the fit of the experimental data in a polynomial equation, which must describe the behavior of a data set with statistical model previsions. Therefore, the combination of CCD and RSM creates a statistical technique for designing experiments, building models, evaluating the effects of several factors, and searching optimum conditions for desirable responses. On the other hand, by this method, the interactions of possible influencing parameters on treatment efficiency can be evaluated with a limited number of planned experiments (Khaloo *et al.* 2015).

Based on the facts mentioned above, in this study a nanocomposite of $NiFe_2O_4$-graphene oxide modified by a poly aminoglycoside (neomycin) was synthesized. Sonochemical nucleophilic substitution reaction was applied to modify the graphene oxide surface by neomycin (Ne). $NiFe_2O_4$ was synthesized by a simple hydrothermal process and was directly loaded on the modified graphene oxide (MGO). The chemical structure of nano-composite was characterized by different techniques such as scanning electron microscopy (SEM), energy dispersive X-ray spectroscopy (EDS), X-ray diffraction (XRD) and Fourier transform infrared (FT-IR) spectroscopy. The synthesized magnetic modified nano-composite (MMNC) were used as nano-adsorbent for removal of 4-nitrophenol (4-NP) in water. The adsorption kinetic and isotherm parameters of the adsorption process were investigated. A three-factor Box–Benhken design coupled with response surface method (BBD-RSM) was applied to evaluate and optimize the important experimental variables and a quadratic model was derived using analysis of variance to predict the effects of different parameters and their interactions on the removal efficiency of MMNC.

MATERIALS AND METHOD

Chemicals and reagent

Ferric chloride hexahydrate, nickel chloride hexahydrate, potassium permanganate, graphite powder, sulfuric acid

(95%), hydrogen peroxide (30%, w/w) and 4-nitrophenol were purchased from Merck (Darmstadt, Germany). Neomycin sulfate was purchased from Sigma-Aldrich Co. All chemicals were of analytical grade and used as received without further purification. De-ionized (DI) water was used as the solvent throughout the experiments. All of the working solutions used for the optimization and establishing the isotherms were prepared by successive dilution of stock solutions.

Synthesis of modified magnetic nano-composite

GO was synthesized from graphite powder by a modified Hummer's method as published previously (Khaloo *et al.* 2016). The synthesized GO 5 mg/ml suspension in ethanol was exfoliated with ultrasonic radiation (Elmasonic E 60 H, 37 kHz 400 W, continuous wave mode, Germany) to prepare graphene oxide nanosheets and also to enhance the chemical reactivity of GO. The color of the particles changes to light brown after 2 hours sonication. Ten millilitres of 30 mg/ml neomycin sulfate was added to the light brown particles to start the chemical reaction of imide bonds formation. The reaction took place in 30 min to develop a black particles suspension. The MGO was centrifuged at 4,000 rpm and washed with DI water three times.

The MMNC was synthesized by functionalization of MGO with nickel ferromagnetic particles by the hydrothermal method. In a typical procedure, the as-prepared MGO (450 mg) was exfoliated by sonication in 60 ml of DI water for 15 min. Then, 25 ml aqueous solution containing 1 g of $FeCl_3.6H_2O$, 0.44 g of $NiCl_2.6H_2O$ (molar ratio of Fe:Ni, 2:1) in 0.4 M HCl was dropped into the MGO suspension at 80 °C followed by stirring for 30 min. After that, the pH of the mixture was adjusted to about 11 by dropping in 1 M NaOH. The mixture was transferred into a 100 ml Teflon-lined stainless steel autoclave and heated at 170 °C for 10 h. A solid black product was obtained and washed several times with DI water. The obtained nano-composite was dried at 50 °C overnight.

The morphology and elemental analysis of the synthesized magnetic nano-particles were assessed by obtaining SEM images, recorded using a Czech Republic MIRA3, TESCAN scanning electron microscope equipped with an EDS accessory. The microscopic properties, such as the crystal structure, the crystal orientation and crystal size of the prepared MMNC samples, were recorded by XRD (D8 Advanced Bruker diffractometer), using Cu Kα radiation with a scanning range of 2θ 10–90°. FT-IR spectra of GO and MMNC were measured with FT-IR spectroscopy (Rayleigh WQF-510A, Beijing, China).

Experimental procedures

Before the development of response surface models, the effects of various parameters such as initial pH, 4-NP concentration, adsorbent dosage and reaction time on adsorption of 4-NP on MMNC were investigated. Batch adsorption experiments were carried out in a 50 ml flask at room temperature (25 ± 2 °C). Typically, an appropriate concentration of 4-NP solution (at the range of 15–100 mg/l) was prepared by diluting the stock solution of 1,000 mg/l. The pH of the 4-NP solution was adjusted to the desired value (between 3.0 and 8.0) using 0.1 M hydrochloric acid and/or 0.1 M sodium hydroxide. An appropriate dosage of MMNC (1.0–5.0 g/l) was mixed with 25 ml 4-NP solution and the mixture was shaken. During each experiment, at certain time intervals, a 1.0 ml sample was withdrawn, adsorbent was removed by using an external magnet and then the residual concentration of 4-NP was measured by a UV–Vis spectrophotometer (AvaSpec-2048, Avantes, The Netherlands) at the lambda max. The removal percent was calculated by the ratio of eliminated values to initial values of 4-NP concentration as:

$$\%\ \text{Removal} = \frac{C_0 - C_t}{C_0} \times 100 \quad (1)$$

where C_0 and C_t are the initial and residual concentration of 4-NP (mg/l).

Experimental design with RSM

Experimental design was based on the Box–Benhken design with three factors in three levels. Table 1 shows the independent variables, experimental ranges, and coded and uncoded levels of the tested variables in the BBD. The 4-NP concentration (X_1), the initial pH (X_2) and MMCN concentration (X_3) were chosen as the independent input variables. The removal efficiency of 4-NP (Y) was used as the dependent output variable. A quadratic polynomial equation was used to fit the response variable:

$$Y = \beta_0 + \sum_{i=1}^{n} \beta_i x_i + \sum_{i=1}^{n} \beta_{ii} x_i^2 + \sum_{i=1}^{n-1} \sum_{j=i+1}^{n} \beta_{ij} x_i x_j \quad (2)$$

Table 1 | Variables levels for the removal of 4-NP by MMNC using BBD-RSM

		Actual values of the levels of the coded variables		
Process variables	**Symbol**	**−1**	**0**	**+1**
4-NP (mg/l)	X_1	30	55	80
pH	X_2	5.0	6.0	7.0
MMNC g/l	X_3	2.0	3.0	4.0

where Y represents the predicted removal efficiency of 4-NP, β_0 is the offset term, β_i are the linear coefficients, β_{ii} are the quadratic coefficients, β_{ij} are the interaction coefficients and x_i and x_j are the independent variables.

All of the experimental results were expressed as mean ± standard deviations of three duplicate measurements. Statistical analysis was performed by using the Minitab 16 software (Minitab Inc., State College, PA, USA) and a second-order polynomial regression model containing the coefficient of linear, quadratic and interaction terms. In order to test the model significance and suitability, the analysis of variance (ANOVA) was performed for each response. The significances of all terms in the polynomial were statistically analyzed by computing the F-value at a probability $p = 0.05$.

RESULTS AND DISCUSSION

Characterization of MMNC

The MMNC was characterized by SEM, equipped with an EDS accessory, and X-ray powder diffraction techniques. An overview of the morphology of graphene oxide, neomycin-modified graphene oxide and MMNC has been shown in Figure 1(a)–1(c), respectively.

As shown, the average thickness of the GO flake measured using SEM is ~2.1 nm and the particle size of $NiFe_2O_4$ particles which have been decorated on GO sheets is less than 20 nm. EDS analysis was performed to determine the elemental composition of the synthesized compounds (Figure 1(a1)–(c1)). The EDS spectrum demonstrated the presence of C, O, N, Ni, and Fe in the structure of MMNC. The C element comes from both graphene nanosheets and neomycin, N comes from neomycin, and O is attributed to both GO and $NiFe_2O_4$ nano-particles n and Si element was present from the plated element for SEM measurement.

The X-ray powder diffraction patterns of the GO and $NiFe_2O_4$-Ne-GO are shown in Figure 2. A sharp diffraction peak at around $2\theta = 10.2^{o}$, which corresponds to (001) plane of GO, and no obvious peak of graphite indicate the formation of GO from graphite. This sharp peak was clearly observed in both XRD patterns. The characteristic peaks at $2\theta = 18.7$, 30.7, 35.5, 38.8, 44.8, 55.6 and 64.3° can be indexed as the (111), (220), (311), (400), (422), (511) and (440) crystal planes of $NiFe_2O_4$, respectively. The XRD pattern of MMNC shows a sharp peak at around 10 that corresponds to the plane of GO, which confirmed that the nano-particles of $NiFe_2O_4$ coated on MGO and MMNC composite were prepared successfully.

FT-IR spectra of graphene oxide, and MMNC have been illustrated in Figure 2(b). C-O stretching vibration of epoxy and alkoxy appeared at 1,046 and 1,220 cm^{-1} and the stretching vibration bands of C=C and C=O were observed at 1,600–1,603 and 1,720 cm^{-1}, respectively. The peaks at 3,100–3,500 cm^{-1} can be attributed to the O-H stretching vibration of carboxyl groups and the adsorbed water molecules and N-H stretching vibration of the amine group of neomycin. The characteristic band at 630 cm^{-1} is assigned to the intrinsic vibration of nickel ferrite and demonstrates that $NiFe_2O_4$ is present and supported on GO in MMNC. The FT-IR spectrum of MMNC shows bands around 2,900 and 2,890 cm^{-1}, which can be attributed to the C-H and C-N stretching vibration. The observed peaks at 1,380 and 1,090 cm^{-1} correspond to the O-H and C-O stretching vibration of alcohol groups and the peaks at 1,275 and 1,150 cm^{-1} correspond to the C-O and C-N stretching vibration of ether and amine groups of neomycin, respectively.

Optimization by response surface method

In order to model second-order effects and determine optimal removal conditions, the RSM with BBD has been used. The primary studies of adsorption behaviour of 4-NP on the surface of MMNC showed that the kinetics of adsorption is relatively fast and the initial pH of solution has a critical role in removal efficiency since it affects the ionization or dissociation of the adsorbate, properties of the adsorbent's surface and, consequently, the interaction between the adsorbent and adsorbate. The initial concentration of 4-NP and dosage of MMNC are the two other parameters affecting the removal efficiency of 4-NP; therefore, these three parameters in three levels have been selected to design the experiments. With three factors the number of design points of the BBD is 12 plus a number of center points, which is 16 in this study. To reduce the error, a random order method was used to conduct the

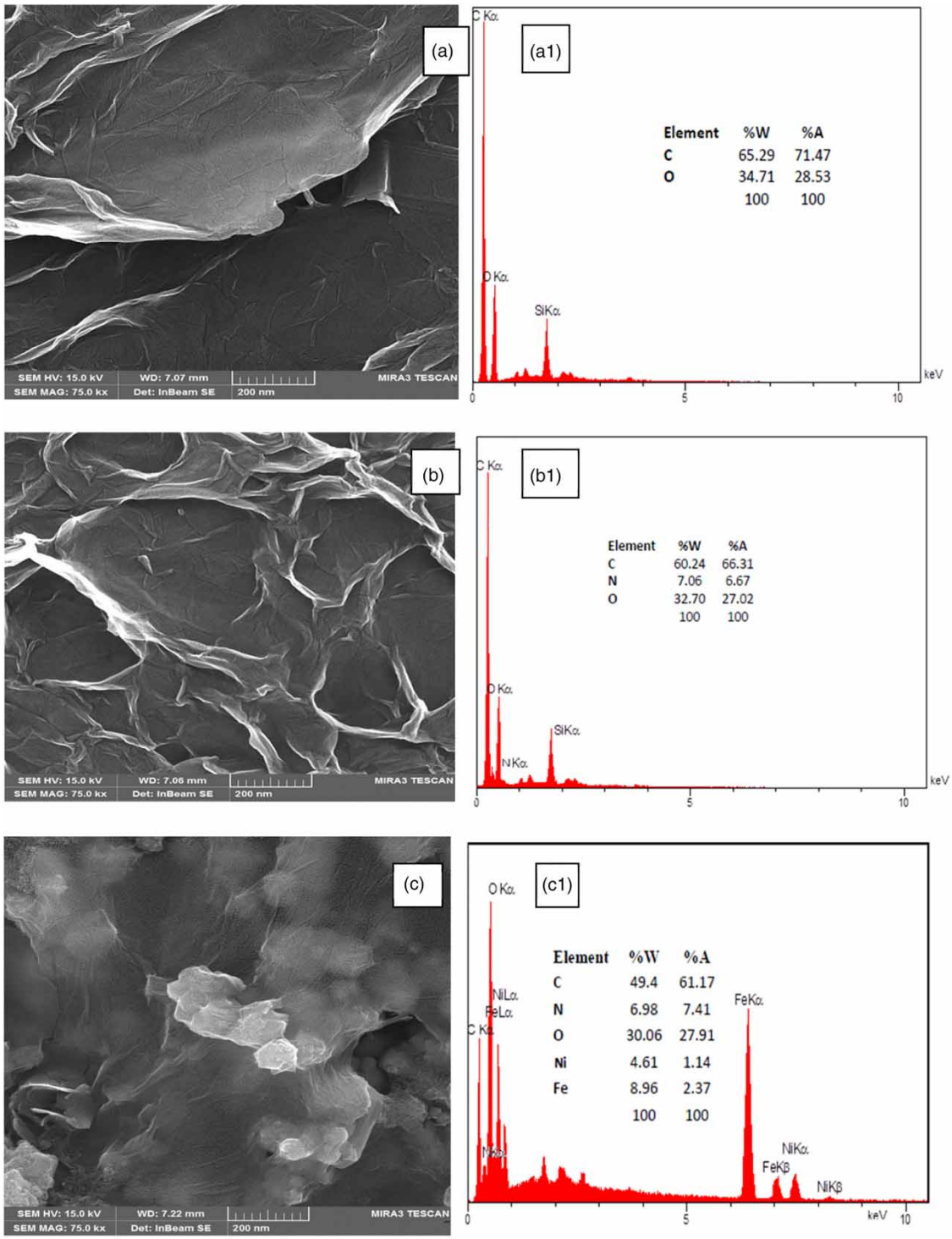

Figure 1 | SEM images of (a) GO, (b) Ne-GO and (c) $NiFe_2O_4$-Ne-GO nano-particles. EDS spectrum of (a1) GO, (b1) Ne-GO and (c1) $NiFe_2O_4$-Ne-GO.

experiments. Table 2 shows experimental factors for each run and the removal efficiency as a corresponding response. A quadratic model has been used to fit the experimental results by software. The validity and significance of parameters have been assessed by ANOVA. The *p*-value lower than 0.05 implies the model or parameters are meaningful at confidence level of 95%. An experimental relationship between the response (removal efficiency) and

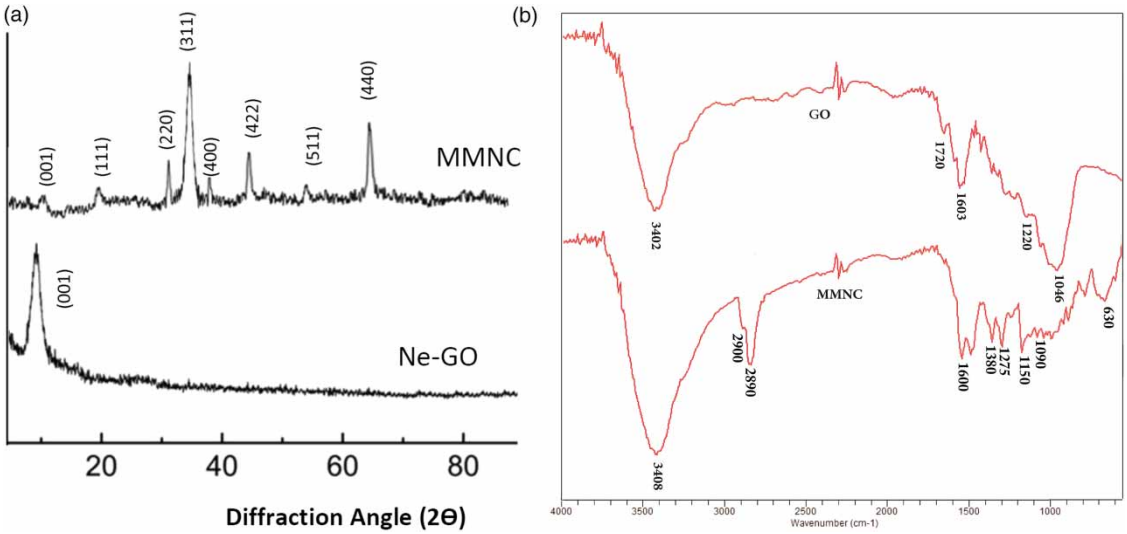

Figure 2 | (a) XRD pattern of modified graphene oxide (Ne-GO) and MMNC and (b) FT-IR spectra of GO and MMNC.

the independent variables was expressed in terms of the quadratic polynomial equation as below:

$$\%\ \text{Removal} = -109.91 + 0.23^{*}\text{NP} + 34.84^{*}\text{MMNC} + 47.17^{*}\ \text{pH} - 0.0067^{*}\text{NP}^{2} - 4.25^{*}\text{MMNC}^{2} - 4.27^{*}\ \text{pH}^{2} - 0.063^{*}\text{NP}^{*}\text{MMNC} + 0.069^{*}\text{NP}^{*}\ \text{pH} + 0.091^{*}\text{MMNC}^{*}\ \text{pH}$$

Table 2 | Experimental design and response of removal of 4-NP

Run	4-NP, mg/l	MMNC, g/l	pH	% Removal
1	55	3	6	93
2	55	2	7	80
3	80	2	5	69
4	30	2	6	81
5	55	3	6	94
6	80	2	7	70
7	80	4	6	86
8	30	3	5	92
9	30	3	7	90
10	80	3	5	77
11	55	3	6	93
12	80	2	6	78
13	55	4	7	91
14	55	3	6	93
15	30	3	5	95
16	55	3	6	93

The estimated parameters to model the removal efficiency of 4-NP on the surface of MMNC are given in Table 3. The results obviously show that the pH of the solution had the most significant effect on the removal efficiency and, after that, the concentration of nano-sorbent had an important role in the model. The combinations of all factors were found to be significant except the interaction of MMNC concentration and pH.

The relationship between the mean square of the model and the error is expressed by the F test and *p*-value. Table 4 presents the results of the ANOVA for the second-order polynomial model. At a confidence level of 95%, the *p*-value for the model, linear, quadratic and interaction terms have a significant effect ($p \leq 0.05$). The high values

Table 3 | Estimated regression coefficients and *p*-values of removal efficiency of 4-NP

Term	Coefficient	SE coefficient	*p*-value
Constant	−109.91	52.00	0.027
NP	0.23	0.43	0.015
MMNC	34.84	10.92	0.015
pH	47.17	14.37	0.013
NP*NP	−0.0067	0.0024	0.040
MMNC*MMNC	−4.25	1.46	0.029
pH*pH	−4.27	1.16	0.008
NP*MMNC	−0.063	0.039	0.015
NP*pH	0.069	0.044	0.016
MMNC*pH	0.091	1.59	0.956

SE: standard error.

Table 4 | Analysis of variance for the removal of 4-NP

Source	DF	Sum of square	F-value	*p*-value
Model	9	1273.52	30.61	0.000
Linear	3	990.25	5.50	0.029
Square	3	253.93	19.23	0.001
Residual error	7	32.36		
Lack-of-fit	2	27.06	12.76	0.11
Pure error	5	5.30		
Total	16	1305.88		

DF: degrees of freedom.

of statistical parameters R^2 (0.9752) and R^2_{adj} (0.9593) signify the good fitting of experimental results to the model. The absence of any lack of fit ($p > 0.05$) also strengthened the reliability of the model. In other words, the proposed model can significantly predict many changes at the level of the response of the regression equation.

In order to improve and analyze multivariate systems, geometric displays, especially two-dimensional and three-dimensional diagrams, are the best. Therefore, response surface graphs (three-dimensional diagrams) for illustrating response (% removal) versus dependent variables (pH, NP, and MMNC) as a function of two factors when the third factor was kept constant at a center point have been shown in Figures 3–5. Figure 3 shows the effect of pollutant concentration and adsorbent dose on the removal efficiency of 4-nitrophenol from aqueous solutions. As is evident from the figure, by increasing the adsorbent dose, the removal efficiency is reduced, and the removal efficiency is reduced by increasing the contaminant concentration. The graph also shows the fact that the two parameters of the concentration of the contaminant and the adsorbent dose interact with each other and the efficiency of the elimination is a function of both parameters. In the range of 30–60 mg/l of the contaminant, the removal efficiency is greater than 90%, with an adsorbent dose of at least 3.0 g/l. As expected, with increasing concentrations of pollutants, since most surface

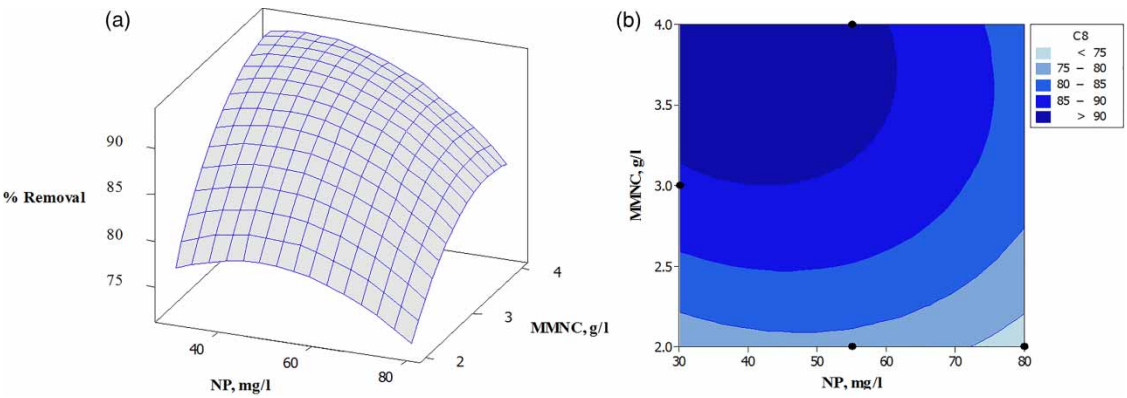

Figure 3 | Response surface (a) and the corresponding contour (b) plots for removal of 4-NP as function MMNC and 4-NP concentration.

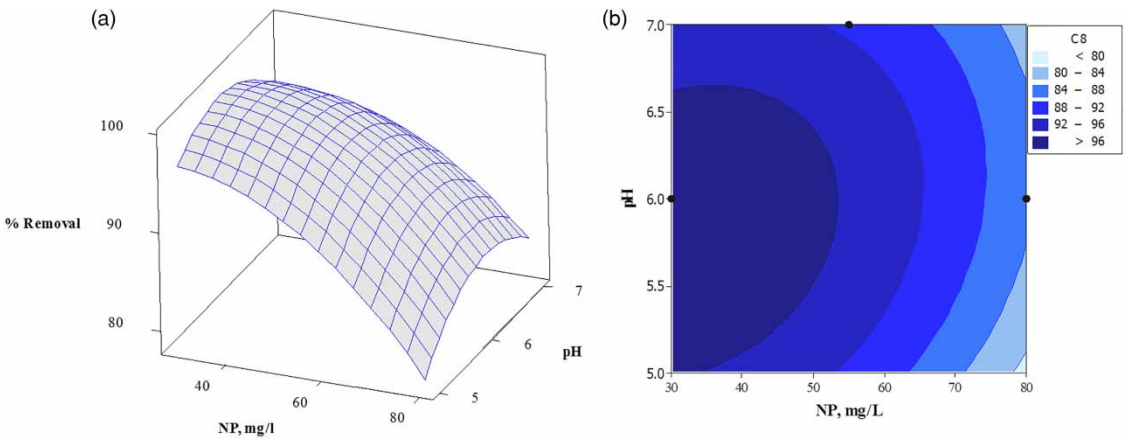

Figure 4 | Response surface (a) and the corresponding contour (b) plots for removal of 4-NP as function of pH and 4-NP concentration.

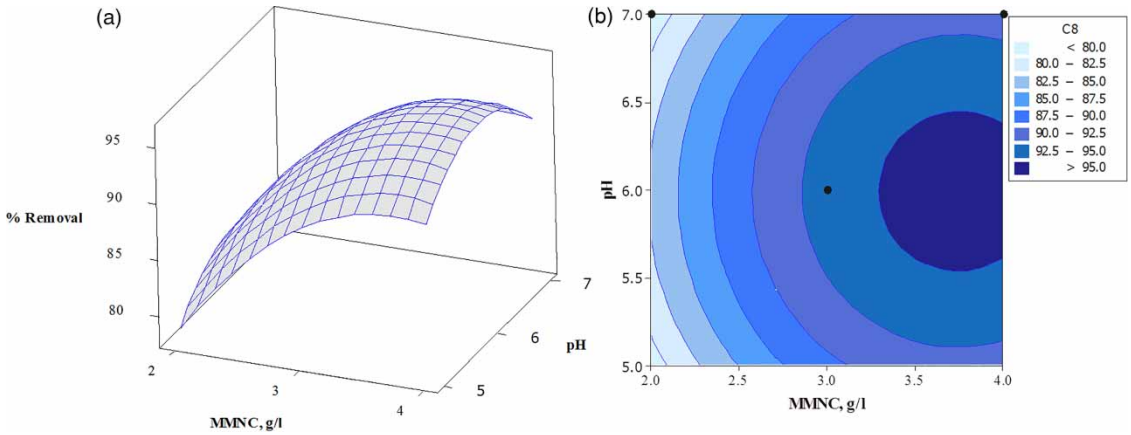

Figure 5 | Response surface (a) and the corresponding contour (b) plots for removal of 4-NP as function of pH and MMNC concentration.

sites are occupied by the pollutant, the efficiency of removal is reduced and, in order to maintain the efficiency of removal, it is necessary to increase the amount of MMNC simultaneously. On the other hand, by using Figure 3(b) the best dosage of adsorbent could be selected according to the pollutant concentration and the desired removal efficiency.

The response surface and the corresponding contour plots of the 4-nitrophenol removal efficiency have been shown against the contaminant concentration and pH of the solution in Figure 4. As is evident from the figure, by increasing the pH of the solution from 5 to 6.5 in the concentration range of 30 to 50 mg/l, the removal efficiency increases and then, by increasing pH, the removal efficiency is reduced. As expected from the chemical structure of the pollutant, with increasing pH, de-protonation of contaminants increases and therefore the negative charge increases. On the other hand, the adsorbent surface possesses a positive charge in acidic and a negative charge in alkaline environments. Therefore, electrostatic repulsion prevents adsorption of 4-NP in alkaline environments and reduces the removal efficiency.

The US EPA has established for 4-nitrophenol the criterion of less than 550 μg/l to protect freshwater aquatic life (US EPA 1980). As Figure 4 shows, the residual level of NP after adsorption will be less than the above-mentioned criterion when its initial concentration is less than 45 mg/l, pH is 5–6.7 and the minimum dose of MMNC is 3.0 g/l. This result confirms the high efficiency of the synthesized MMNC in the adsorptive removal of 4-NP.

According to Figure 5 by increasing the adsorbent dose in the range of 3.5 to 4 g/l and pH from 5.6 to 6.6, the removal efficiency higher than 95% is achieved. Thus, at all concentrations, the best removal efficiency is achieved at pH 6. By increasing the acidity of the solution, as a result of the simultaneous protonation of the adsorbent and the contaminant, the electrostatic repulsion increases and consequently the removal efficiency is reduced. At pH values higher than pK_a of 4-NP, the same trend of increasing negative charge resulting from de-protonation of contaminants and adsorbent surface reduces removal efficiency. Such a trend of surface charge changes is only pH-dependent and is present in all adsorbent dosages. Therefore, the dosage of adsorbent and pH of the environment do not have a significant effect on each other. The results of the ANOVA in Table 3 also confirm the insignificant interaction of these two independent parameters (MMNC*pH p-value is 0.954).

The optimum parameters for high removal efficiency of 4-NP as specified by RSM are initial contaminant concentration 60 mg/l, pH 6 and adsorbent dose 3 g/l. Based on the predictive model, removal efficiency of 4-NP at the optimum condition was calculated as 94.8%. Experimental removal of 93.3% matches quite well with the predicted one, which validated the RSM models with good correlations ($R^2 = 0.9897$). On the other side, response surface graphs and their corresponding contour help to find the optimum parameters to get the desired removal efficiency according to the other parameters.

Isotherm study of the adsorption process

After the optimization, adsorption isotherm studies were conducted at room temperature under the optimized conditions to evaluate the mechanism of adsorption process for the removal of 4-NP. Langmuir and Freundlich models

were used for modeling:

$$\text{Original form of Langmuir equation: } q_e = \frac{bq_mC_e}{1+bC_e} \quad (3)$$

$$\text{Freundlich equation: } q_e = K_fC^{\frac{1}{n}} \quad (4)$$

The sorption capacity, q_t, the number of ions adsorbed per mass unit of adsorbent, (in milligram of pollutant per gram of sorbent) was calculated using the following equation:

$$q_t = \frac{(C_0 - C_t)V}{m} \quad (5)$$

In the above equations, C_0 and C_e denote the initial and equilibrium concentration of the adsorbate (mg/l), respectively. q_t and q_e are the temporary and equilibrium loading of sorbate on sorbent (mg/g), q_m and b are the Langmuir constants related to the maximum adsorption capacity (mg/g), and the relative energy of adsorption (l/mg), respectively. K_f and n are the Freundlich constants related to adsorption capacity and adsorption intensity, respectively. V is the volume of the solution (l) and m is the weight of sorbent (g).

Figure 6 shows the adsorption isotherm of the process using Langmuir and Freundlich models. The isotherm parameters which have been derived from both models have been given in Table 5. As can be concluded from data of the table, the most precise match was acquired using the Langmuir model. Hence, this confirmed that the adsorption of 4-NP is a monolayer adsorption process on a surface containing a finite number of identical sites. Table 5 also shows that the presence of neomycin on the surface of the magnetic nano-particle improves the maximum absorbance capacity by up to 28%. The maximum

Table 5 | Isotherm parameters of the adsorption process on the surface of MMNC and $NiFe_2O_4$-GO

	Langmuir			Freundlich		
Sorbent	q_m (mg/g)	b (l/mg)	R^2	K_f	n	R^2
MMNC	125.6	0.064	0.9929	3.57	0.96	0.9410
$NiFe_2O_4$-GO	98.7	0.056	0.9987	3.21	0.87	0.9395

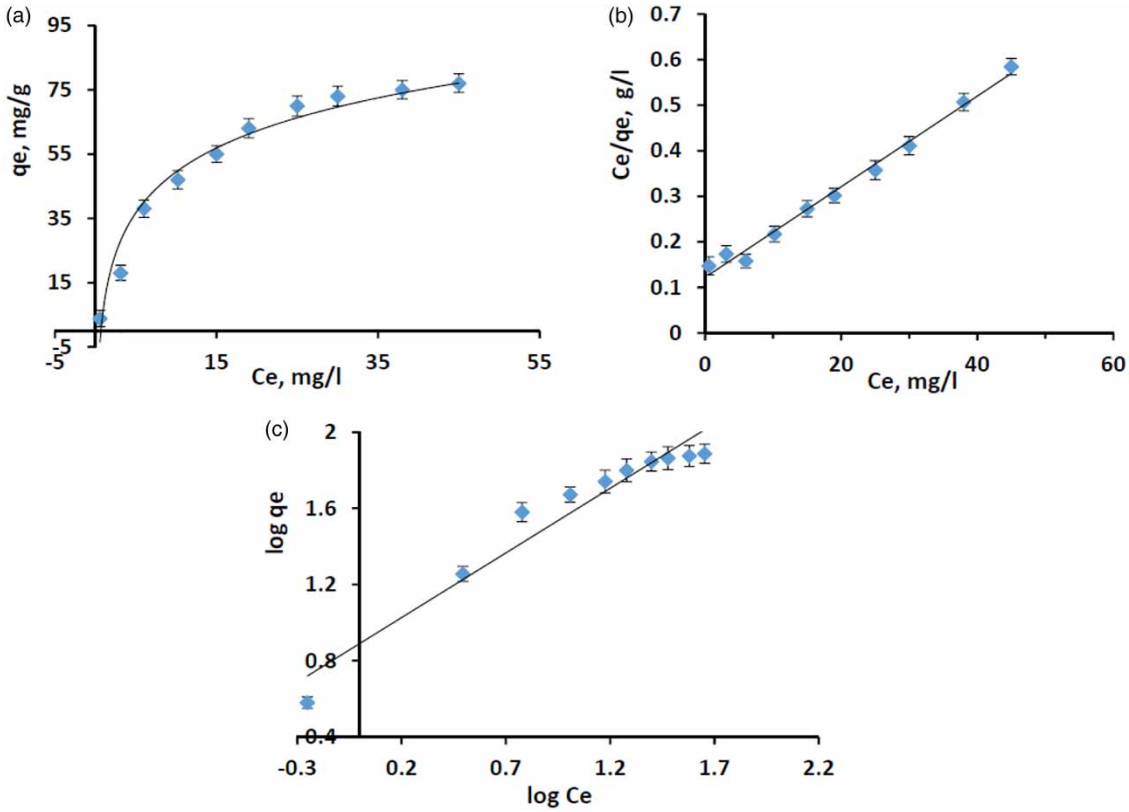

Figure 6 | Adsorption isotherms for removal of 4-NP using MMNC: (a) Langmuir model, (b) linearized Langmuir and (c) Freundlich model.

adsorptive capacity of magnetic modified graphene oxide was found to be 125.6 mg of NP/g sorbent which was comparable or higher in some cases to the other reported sorbents for removal of NP (Table 6). Neomycin provides several amine, alcohol and ether groups at the surface of GO and then different interactions, such as electrostatic interaction and hydrogen bonding, could improve adsorption efficiency of 4-NP on the surface of MMNC (Lu *et al.* 2017).

Kinetic study of the adsorption process

In order to study the kinetic variables of the adsorption process of 4-NP using MMNC the pseudo-first-order and pseudo-second-order kinetic models were used:

$$\mathrm{Log}(q_e - q_t) = \mathrm{Log}\, q_e - \frac{K_1 t}{2.303} \tag{6}$$

$$\frac{t}{q_t} = \frac{1}{K_2 q_e^2} + \frac{t}{q_e} \tag{7}$$

In the above equations, q_e and q_t denote the sorption capacity (mg/g) at equilibrium and time t, respectively. K_1 (min^{-1}) and K_2 (gg/(mg·min)) are the pseudo-first- and the pseudo-second-order constants. Figure 7 illustrates the kinetic studies of 4-NP adsorption on MMNC according to the above-mentioned equations. The kinetic parameters

Table 6 | Literature review of recently published reports on adsorption removal of 4-nitrophenol

Adsorbent	q_m (mg/g)	pH, Sorbent dose, Equilibrium time	Reference
Activated carbon from peach stones and treated with urea	234.0	pH = ND, 2.4 g/l, 4 h	Álvarez-Torrellas *et al.* (2017)
Metal–organic framework (Cr-BDC)	19.0	pH = 6, 0.2 g/l, 24 h	Chen *et al.* (2017)
Fe-nano zeolite	223.1	pH = 5, 5.0 g/l, 3 h	Huong *et al.* (2016)
Amino MIL-53 Al	297.85	pH = ND, 2.0 g/l, 48 h	Jia *et al.* (2017)
MWCNT/iron oxide/β-CD	33.34	pH = 7, 1.4 g/l, 3 h	Liu *et al.* (2014)
Magnetic alginate beads	140.0	pH = 6.5, 107.5 g/l, 1 h	Obeid *et al.* (2015)
β-CD @silica gel	41.5	pH = 8, 10.0 g/l, 2 h	Shen *et al.* (2015)
Nano-zeolite	156.6	pH = 6, 5.0 g/l, 2.5 h	Pham *et al.* (2016)
Ni-Al DLH	77.7	pH = 7, 0.1 g/l, 24 h	Sun *et al.* (2015)
Gemini modified montmorillonites	81.30	pH = 10, 4.0 g/l, 3 h	Xue *et al.* (2013)
Fe_3O_4-PSS@ZIF-67	52.50	pH = 5, 0.7 g/l, 2 h	Yang *et al.* (2018)
$NiFe_2O_4$-Ne-GO	125.4	pH = 6, 3.0 g/l, 0.7 h	This work

Cr-BDC: chrome-benzenedicarboxylates, CD: cyclodextrin, MWCNT: multi-walled carbon nanotube, DLH: double layered hydroxides, PSS: poly (sodium-p-styrenesulfonate), ND: not determined.

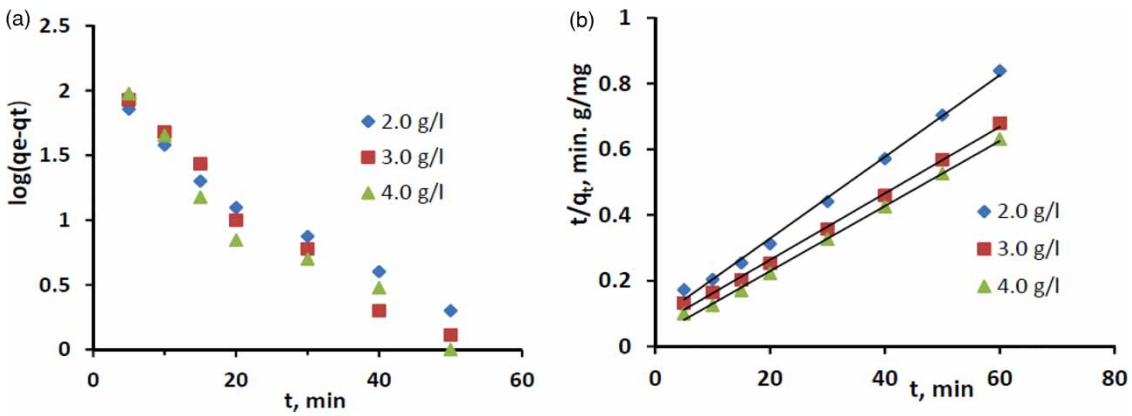

Figure 7 | (a) Pseudo-first-order and (b) pseudo-second-order kinetics of sorption of 4-NP at three different dosages of MMNC and optimum conditions.

Table 7 | Kinetic parameters of adsorption of 4-NP at three different dosages of MMNC (2.0, 3.0 and 4.0 g/l)

	Pseudo-first-order			Pseudo-second-order		
Parameter	**2.0**	**3.0**	**4.0**	**2.0**	**3.0**	**4.0**
q_{cal}	58.9	70.4	72.1	80.6	90.1	101.4
K_1 (min^{-1})	0.087	0.11	0.12	–	–	–
K_2 (gg/(mg·min))	–	–	–	1.9×10^{-3}	1.7×10^{-3}	3.1×10^{-3}
R^2	0.9670	0.9580	0.9176	0.9960	0.9971	0.9978

that were evaluated from the slope and intercepts of the graphs are summarized in Table 7. The values of the correlation coefficients proved that the pseudo-second-order adsorption model is more suitable to describe the adsorption kinetics of 4-NP on the surface of MMNC.

CONCLUSION

In this study, $NiFe_2O_4$-Ne-GO was synthesized as a new nano-composite adsorbent. The synthesized nano-adsorbent was characterized by SEM, EDS and XRD techniques. The applicability of the synthesized nano-composite was assessed for adsorption removal of 4-nitrophenol as a representative of the phenolic pollutants. The adsorption process has fast kinetics so that more than 95% of absorption occurs in the first 40 minutes of contact. RSM coupled with BBD was used for the optimization of the operation parameters for the adsorption removal of 4-NP. Response surface curves showed that the synthesized MMNC in the removal of 4-NP has excellent adsorption capability in such a way that the residual level of 4-NP after adsorption will be less than the criterion to protect freshwater aquatic life (550 μg/l). Thus, this adsorptive system can be introduced as a new sorbent for the removal of phenolic compounds from aqueous environments in mixing tank reactors, continuous-flow or intermittent flow.

ACKNOWLEDGEMENTS

The authors gratefully acknowledge the support of this work by the Shahid Beheshti University of Medical Sciences.

CONFLICT OF INTEREST

The authors have declared no conflict of interest.

REFERENCES

Abd Manan, T. S. B., Khan, T., Sivapalan, S., Jusoh, H., Sapari, N., Sarwono, A., Ramli, R. M., Harimurti, S., Beddu, S., Sadon, S. N., Kamal, N. L. M. & Malakahmad, A. 2019 Application of response surface methodology for the optimization of polycyclic aromatic hydrocarbons degradation from potable water using photo-Fenton oxidation process. *Science of the Total Environment* **665**, 196–212.

Abtahi, M., Koolivand, A., Dobaradaran, S., Yaghmaeian, K., Mohseni-Bandpei, A., Khaloo, S. S., Jorfi, S. & Saeedi, R. 2017 Defluoridation of synthetic and natural waters by polyaluminum chloride-chitosan (PACl-Ch) composite coagulant. *Water Science & Technology: Water Supply* **18** (1), 259–269.

Adesina, O. A., Abdulkareem, F., Yusuff, A. S., Lala, M. & Okewale, A. 2019 Response surface methodology approach to optimization of process parameter for coagulation process of surface water using *Moringa oleifera* seed. *South African Journal of Chemical Engineering* **28**, 46–51.

Altowayti, W. A. H., Algaifi, H. A., Bakar, S. A. & Shahir, S. 2019 The adsorptive removal of As(III) using biomass of arsenic resistant *Bacillus thuringiensis* strain WS3: characteristics and modelling studies. *Ecotoxicology and Environmental Safety* **172**, 176–185.

Álvarez-Torrellas, S., Martin-Martinez, M., Gomes, H. T., Ovejero, G. & García, J. 2017 Enhancement of p-nitrophenol adsorption capacity through N_2-thermal-based treatment of activated carbons. *Applied Surface Science* **414**, 424–434.

Chen, J., Sun, X., Lin, L., Dong, X. & He, Y. 2017 Adsorption removal of o-nitrophenol and p-nitrophenol from wastewater by metal–organic framework Cr-BDC. *Chinese Journal of Chemical Engineering* **25** (6), 775–781.

Chu, T. P. M., Nguyen, N. T., Vu, T. L., Dao, T. H., Dinh, L. C., Nguyen, H. L., Hoang, T. H., Le, T. S. & Pham, T. D. 2019 Synthesis, characterization, and modification of alumina nanoparticles for cationic dye removal. *Materials* **12** (3), 450.

Gadekar, M. R. & Ahammed, M. M. 2019 Modelling dye removal by adsorption onto water treatment residuals using combined response surface methodology-artificial neural network approach. *Journal of Environmental Management* **231**, 241–248.

Gholami, M., Abbasi Souraki, B., Pendashteh, A., Pourkarim Mozhdehi, S. & Bagherian Marzouni, M. 2017 Treatment of pulp and paper wastewater by lab-scale

coagulation/SR-AOPs/ultrafiltration process: optimization by Taguchi. *Desalination and Water Treatment* **95**, 96–108.

Hu, Z., Qin, S., Huang, Z., Zhu, Y., Xi, L. & Li, Z. 2017 Recyclable graphene oxide-covalently encapsulated magnetic composite for highly efficient Pb(II) removal. *Journal of Environmental Chemical Engineering* **5** (5), 4630–4638.

Huong, P.-T., Lee, B.-K., Kim, J. & Lee, C.-H. 2016 Nitrophenols removal from aqueous medium using Fe-nano mesoporous zeolite. *Materials & Design* **101**, 210–217.

Jia, Z., Jiang, M. & Wu, G. 2017 Amino-MIL-53(Al) sandwich-structure membranes for adsorption of p-nitrophenol from aqueous solutions. *Chemical Engineering Journal* **307**, 283–290.

Kaur, M., Kaur, M. & Sharma, V. K. 2018 Nitrogen-doped graphene and graphene quantum dots: a review on synthesis and applications in energy, sensors and environment. *Advances in Colloid and Interface Science* **259**, 44–64.

Kefeni, K. K., Mamba, B. B. & Msagati, T. A. M. 2017 Application of spinel ferrite nanoparticles in water and wastewater treatment: a review. *Separation and Purification Technology* **188**, 399–422.

Khaloo, S. S. & Fattahi, S. 2014 Enhancing decolorization of eriochrome blue black R during nano-size zero-valent iron treatment using ultrasonic irradiation. *Desalination and Water Treatment* **52** (16–18), 3403–3410.

Khaloo, S. S., Zolfaghari, H. & Gholamnia, R. 2015 Response surface methodology for optimization of 4-nitrophenol degradation by a heterogeneous Fenton-like reaction on nano-zero-valent iron. *Desalination and Water Treatment* **56** (8), 2206–2213.

Khaloo, S. S., Ahmadi Marzaleh, M., Kavousian, M. & Bahramzadeh Gendeshmin, S. 2016 Graphene oxide coated wad as a new sorbent in fixed bed column for the removal of crystal violet from contaminated water. *Separation Science and Technology* **51** (1), 1–10.

Li, N., Jiang, H.-L., Wang, X., Wang, X., Xu, G., Zhang, B., Wang, L., Zhao, R.-S. & Lin, J.-M. 2018 Recent advances in graphene-based magnetic composites for magnetic solid-phase extraction. *TrAC Trends in Analytical Chemistry* **102**, 60–74.

Liu, W., Jiang, X. & Chen, X. 2014 A novel method of synthesizing cyclodextrin grafted multiwall carbon nanotubes/iron oxides and its adsorption of organic pollutant. *Applied Surface Science* **320**, 764–771.

Liu, G., Li, L., Xu, D., Huang, X., Xu, X., Zheng, S., Zhang, Y. & Lin, H. 2017 Metal–organic framework preparation using magnetic graphene oxide–β-cyclodextrin for neonicotinoid pesticide adsorption and removal. *Carbohydrate Polymers* **175**, 584–591.

López-Ortiz, C. M., Sentana-Gadea, I., Varó-Galvañ, P. J., Maestre-Pérez, S. E. & Prats-Rico, D. 2018 Effect of magnetic ion exchange (MIEX®) on removal of emerging organic contaminants. *Chemosphere* **208**, 433–440.

Lu, Z., Yu, J., Zeng, H. & Liu, Q. 2017 Polyamine-modified magnetic graphene oxide nanocomposite for enhanced selenium removal. *Separation and Purification Technology* **183**, 249–257.

Naddafi, K., Rastkari, N., Nabizadeh, R., Saeedi, R., Gholami, M. & Sarkhosh, M. 2016 Adsorption of 2,4,6-trichlorophenol from aqueous solutions by a surfactant-modified zeolitic tuff: batch and continuous studies. *Desalination and Water Treatment* **57** (13), 5789–5799.

Nasseri, S., Ebrahimi, S., Abtahi, M. & Saeedi, R. 2018 Synthesis and characterization of polysulfone/graphene oxide nano-composite membranes for removal of bisphenol A from water. *Journal of Environmental Management* **205**, 174–182.

Obeid, L., Kolli, N. E., Talbot, D., Welschbillig, M. & Bée, A. 2015 Influence of a cationic surfactant on adsorption of p-nitrophenol by a magsorbent based on magnetic alginate beads. *Journal of Colloid and Interface Science* **457**, 218–224.

Pedersen, N. L., Nikbakht Fini, M., Molnar, P. K. & Muff, J. 2018 Synergy of combined adsorption and electrochemical degradation of aqueous organics by granular activated carbon particulate electrodes. *Separation and Purification Technology*. **208**, 51–58.

Pham, T.-H., Lee, B.-K. & Kim, J. 2016 Improved adsorption properties of a nano zeolite adsorbent toward toxic nitrophenols. *Process Safety and Environmental Protection* **104** (Part A), 314–322.

Pham, T., Bui, T., Nguyen, V., Bui, T., Tran, T., Phan, Q. & Hoang, T. 2018 Adsorption of polyelectrolyte onto nanosilica synthesized from rice husk: characteristics, mechanisms, and application for antibiotic removal. *Polymers* **10** (2), 220.

Pham, T. D., Tran, T. T., Le, V. A., Pham, T. T., Dao, T. H. & Le, T. S. 2019 Adsorption characteristics of molecular oxytetracycline onto alumina particles: the role of surface modification with an anionic surfactant. *Journal of Molecular Liquids* **287**, 110900.

Rashidi Nodeh, H., Sereshti, H., Zamiri Afsharian, E. & Nouri, N. 2017 Enhanced removal of phosphate and nitrate ions from aqueous media using nanosized lanthanum hydrous doped on magnetic graphene nanocomposite. *Journal of Environmental Management* **197**, 265–274.

Saedi, Z. & Roushani, M. 2018 Influence of amine group on the adsorptive removal of basic dyes from water using two nanoporous isoreticular Zn(II)-based metal organic frameworks. *Journal of Nanochemistry Research* **3** (1), 99–108.

Sharma, S. & Simsek, H. 2020 Sugar beet industry process wastewater treatment using electrochemical methods and optimization of parameters using response surface methodology. *Chemosphere* **238**, 124669.

Sharma, K., Dutta, V., Sharma, S., Raizada, P., Hosseini-Bandegharaei, A., Thakur, P. & Singh, P. 2019 Recent advances in enhanced photocatalytic activity of bismuth oxyhalides for efficient photocatalysis of organic pollutants in water: a review. *Journal of Industrial and Engineering Chemistry* **78**, 1–20.

Shen, H.-M., Zhu, G.-Y., Yu, W.-B., Wu, H.-K., Ji, H.-B., Shi, H.-X., She, Y.-B. & Zheng, Y.-F. 2015 Fast adsorption of p-nitrophenol from aqueous solution using β-cyclodextrin grafted silica gel. *Applied Surface Science* **356**, 1155–1167.

Sherlala, A. I. A., Raman, A. A. A., Bello, M. M. & Asghar, A. 2018 A review of the applications of organo-functionalized magnetic graphene oxide nanocomposites for heavy metal adsorption. *Chemosphere* **193**, 1004–1017.

Silva, P. M. O., Raulino, G. S. C., Vidal, C. B. & Nascimento, R. F. d. 2017 Selective precipitation of Cu^{2+}, Zn^{2+} and Ni^{2+} ions using H_2S(g) produced by hydrolysis of thioacetamide as the precipitating agent. *Desalination and Water Treatment* **95**, 220–226.

Sivagami, K., Sakthivel, K. P. & Nambi, I. M. 2018 Advanced oxidation processes for the treatment of tannery wastewater. *Journal of Environmental Chemical Engineering* **6** (3), 3656–3663.

Sun, Y., Zhou, J., Cai, W., Zhao, R. & Yuan, J. 2015 Hierarchically porous NiAl-LDH nanoparticles as highly efficient adsorbent for p-nitrophenol from water. *Applied Surface Science* **349**, 897–903.

US Environmental Protection Agency 2017 *Integrated Risk Information System*. Available from: https://cfpub.epa.gov/ncea/iris/iris_documents/documents/subst/0484_summary.pdf.

US EPA 1980 *Ambient Water Quality Criteria for Nitrophenols*. Criteria and Standards Division, US Environmental Protection Agency, Washington, DC. EPA-440/5-80-063. 2019.

William, W. A., Messai, A. M. & Penny, P. G. 2017 Phenolic compounds in water: sources, reactivity, toxicity and treatment methods. In: *Phenolic compounds – natural sources, importance and applications* (M. Soto-Hernandez, M. Palma-Tenango & M. García-Mateos, eds). IntechOpen, DOI: 10.5772/66927. Available from: https://www.intechopen.com/books/phenolic-compounds-natural-sources-importance-and-applications/phenolic-compounds-in-water-sources-reactivity-toxicity-and-treatment-methods.

Xue, G., Gao, M., Gu, Z., Luo, Z. & Hu, Z. 2013 The removal of p-nitrophenol from aqueous solutions by adsorption using gemini surfactants modified montmorillonites. *Chemical Engineering Journal* **218**, 223–231.

Yang, L., Hu, J., He, L., Tang, J., Zhou, Y., Li, J. & Ding, K. 2017 One-pot synthesis of multifunctional magnetic N-doped graphene composite for SERS detection, adsorption separation and photocatalytic degradation of Rhodamine 6G. *Chemical Engineering Journal* **327**, 694–704.

Yang, Q., Lu, R., Ren, S., Zhou, H., Wu, Q., Zhen, Y., Chen, Z. & Fang, S. 2018 Magnetic beads embedded in poly (sodium-p-styrenesulfonate) and ZIF-67: removal of nitrophenol from water. *Journal of Solid State Chemistry* **265**, 200–207.

First received 15 May 2019; accepted in revised form 14 November 2019. Available online 27 November 2019